Emiss. Control Sci. Technol. (2016) 2:75–88
DOI 10.1007/s40825-016-0033-3

Characterization of Real-Time Particle Emissions from a Gasoline Direct Injection Vehicle Equipped with a Catalyzed Gasoline Particulate Filter During Filter Regeneration

Tak W. Chan[1] · Meghdad Saffaripour[2] · Fengshan Liu[2] · Jill Hendren[1] · Kevin A. Thomson[2] · Joseph Kubsh[3] · Rasto Brezny[3] · Greg Rideout[1]

Received: 30 September 2015 / Revised: 11 December 2015 / Accepted: 3 January 2016 / Published online: 5 February 2016

Abstract Real-time solid particle number (PN), size distributions, black carbon (BC), and particulate matter (PM) mass measurements were obtained from a gasoline direct injection (GDI) vehicle with and without a catalyzed gasoline particulate filter (GPF) over the US Federal Test Procedure 75 (FTP-75) and US06 Supplemental Federal Test Procedure (US06) drive cycles. The organic and elemental carbon fractions of the carbonaceous PM and transmission electron microscope (TEM) images for the exhaust particles were examined. Particles emitted from the GDI vehicle over various moderate driving conditions have similar morphology, size, and composition. These accumulation mode particles have diameters of 50 to 90 nm, have comparable fractal structures to diesel particles, and contain mostly BC with little organic materials. Under aggressive driving conditions, many nanoparticles (<20 nm in diameter) are emitted with the accumulation mode particles. Over the FTP-75 driving conditions, the optimized GPF reaches particle filtration efficiency of over 90 % from clean condition rapidly and filtration efficiency remains unchanged as filter regeneration was not observed. Over the US06 driving condition, filter regeneration was triggered by the high exhaust temperature during which many nanoparticles with diameters smaller than 30 nm are formed downstream of the GPF. TEM image analysis suggests that BC particles collected during the filter regeneration contain a layer of semi-volatile materials on the aggregate surface while the nanoparticles were semi-volatile in nature. During filter regeneration, moderate filtration of the accumulation mode BC particles was still observed.

Keywords Gasoline particulate filter · Regeneration · Direct injection · Soot · Nanoparticles

1 Introduction

Particles originated from incomplete combustion in internal combustion engines are one of the anthropogenic sources that contribute to atmospheric particles. These particles could contain both non-volatile and volatile components and have direct and indirect influences on climate forcing and visibility, as well as adverse health effects [1–3]. In North America at the moment, light-duty vehicles are typically comprised of gasoline port fuel injection (PFI) vehicles. PFI engines inject fuel into the air intake port where the fuel is vaporized and mixed with the intake air to create a premixed homogeneous fuel mixture before entering the cylinders and undergo combustion. When operating under standard ambient condition, premixed combustion in PFI engines generally produces lower levels of particulate matter (PM) and soot emissions than the emissions from direct injection diesel engines. To meet more stringent greenhouse gas (GHG) emission standards, vehicle manufacturers are introducing more fuel-efficient

Electronic supplementary material The online version of this article (doi:10.1007/s40825-016-0033-3) contains supplementary material, which is available to authorized users.

✉ Tak W. Chan
tak.chan@canada.ca

[1] Emissions Research and Measurement Section, Air Quality Research Division, Environment Canada, 335 River Road, Ottawa, Ontario K1A 0H3, Canada

[2] Measurement Science and Standards, National Research Council Canada, 1200 Montreal Road, Ottawa K1A 0R6, Canada

[3] Manufacturers of Emission Controls Association, 2200 Wilson Boulevard, Suite 310, Arlington, VA 22201, USA

gasoline direct injection (GDI) vehicles. The biggest modification in GDI engine compared to traditional PFI engine is that fuel is directly injected into the cylinders after air is compressed or during the compression stroke. The new fuel injection offers less fuel pumping loss, more precise and flexible fuel volume and injection-timing control, higher compression ratio, more charge cooling, and improved combustion efficiency [4, 5]. However, GDI engines were also observed to have higher PM emissions compared to PFI engines due to possible fuel impingement on the piston and cylinder walls, incomplete fuel evaporation, and the inhomogeneity of air fuel mixture [6–8]. PM emission mitigation options for GDI engines do exist, which include engine optimization (e.g., adjusting fuel injection timing and volume, number of fuel injections, fuel injection pressure, injector placement) [9, 10], changing fuel property and composition (e.g., controlling heavy aromatic hydrocarbons, increasing oxygenates in fuel) [11–15], and the use of emission control devices (e.g., gasoline particulate filter (GPF)) [8, 16–19].

Diesel particulate filter (DPF) is the most effective emission control device for reducing PM emissions from diesel engines [20, 21]. Typically, characteristics of a DPF (e.g., filtration efficiency, pressure drops, etc.) are highly dependent upon the filter substrate parameters, such as substrate cell density, porosity, pore size, wall thickness, and washcoat catalysts. However, gasoline exhaust properties and compositions are very different from those of diesel engines, and thus, DPF technology cannot be directly applied to GDI engines without making adjustments to the filter parameters. Saito et al. [16] provided a summary of the major factors that affect GPF performance. For example, most of the particle filtration in a wall-flow DPF is attributed to the presence of a layer of soot which itself acts as a filtration medium [22]. The much lower PM emissions from GDI engines compared to diesel engines could lead to a longer GPF conditioning time, and a thinner soot layer also lowers the particle filtration efficiency of the GPF. A lower pressure drop across the GPF due to a thinner soot layer can be an advantage of not causing additional vehicular fuel consumption, but the pressure drop across the GPF can be increased due to the higher exhaust temperatures and larger exhaust flow rates in gasoline engines compared to diesel engines with comparable displacement. Another important consideration is the need for filter regeneration, which is a combustion mechanism to remove all the accumulated carbonaceous materials (i.e., soot) in the filter to avoid clogging and the buildup of the exhaust back pressure. In the extreme case, heavily accumulated soot in a filter can lead to exceptionally high back pressures which could trigger spontaneous and uncontrolled filter regenerations creating very high temperatures. The extreme thermal shock in certain cases could damage and crack or even melt the filter substrate.

The excess oxygen available in diesel exhaust and the availability of NO for NO_2 conversion provide the needed components to oxidize the accumulated soot during regeneration provided that a certain level of exhaust temperature can be achieved. Gasoline engines typically operate under stoichiometric conditions when air to fuel ratio is continuously monitored and adjusted to ensure all oxygen in the intake air is consumed by the combustion of the injected fuel. This optimizes the performance of the three-way catalytic converter (TWC) to reduce emissions of carbon monoxide (CO), total hydrocarbons (THC), and oxides of nitrogen (NO_x). It is only during decelerations and fuel cuts when excess oxygen is available for GPF regeneration to occur [16]. In some situations, catalysts are added to a GPF in the form of a washcoat to provide certain application benefits. The presence of a catalyst lowers the temperature required for filter regeneration and also enhances the soot oxidation process [23, 24]. Certain catalysts can also extend the performance of the TWC and provide further reductions to the concentrations of CO, THC, and NO_x.

Filter regeneration is a very complex process because the emissions observed during such an event can be attributed to a variety of factors. Many studies have reported elevated emissions of nanoparticles during DPF regeneration [20, 21]. Chemical analysis conducted in some studies suggested that the nanoparticles generated during regeneration are mainly caused by the condensation of volatile materials, but a small number of these nanoparticles can be attributed to the nonvolatile metal particles originated from the additives in lubrication oil [20, 25]. The catalyzed filter has the potential to oxidize gas phase sulfur dioxide (SO_2; which is originated from the sulfur in the fuel) to form sulfur trioxide (SO_3). SO_3 can further combine with water vapor to form sulfuric acid vapor and nucleate downstream of the filter forming nanoparticles [26–28]. For catalyzed filters, certain catalysts may deliver active oxygen species to the soot and promote rapid soot oxidation. The rapid regeneration could result in the breakage of the pre-deposited soot aggregates. While the small particles could be captured by rapid diffusion, fragmentation of aggregates with the more penetrating sizes could pass through the substrate pores when the soot layer is removed according to the filtration theory. Oxidation continues to occur on the aggregates that pass through the substrate pores, and the less reactive part surviving the process eventually contributes to the particle emissions downstream of the filter [23, 29], explaining the reduction of particle filtration efficiency for soot particles during and right after filter regeneration [17, 30].

At the moment, GPF is not a standard emission control device on gasoline vehicles. However, GPF could become an option for lowering PM emissions from some GDI vehicles in the future. As the filter regeneration has such important implications to tailpipe emissions, it is important to properly characterize the PM emissions before, during, and after filter regeneration. In this study, a number of real-time instruments were deployed to measure the emissions (of solid particle number, number size distributions, refractory, and total particle mass) over two standard driving cycles to gain insights

into how moderate and aggressive driving conditions could impact the GPF PM filtration efficiency and how the presence of the GPF affects the exhaust emissions. Off-line analyses were also conducted which include the determination of the organic and elemental fraction of the carbonaceous mass and TEM image analysis of the collected particles.

The complete analysis of the TEM images is given in Saffaripour et al. [31], which showed that GDI soot particles have similar fractal aggregate characteristics when compared with diesel soot particles. Analysis showed that the various driving conditions (e.g., US06 vs. FTP-75) and engine states (e.g., cold vs. warmed engine) have minor impact on the GDI soot particle morphology. These observations imply that a soot layer can be developed over time in a GPF which improves the particle filtration efficiency if there is no filter regeneration. The TEM image analysis also showed evidence of the emissions of semi-volatile materials over the US06 drive cycle with the GPF installed. It is hypothesized that these semi-volatile materials were originated from the filter regeneration and these observations will be shown to be consistent with the real-time particle measurements. In this article, focus is devoted to the analysis and discussion of the various real-time particle measurements to explain the emission characteristics during filter regeneration and provide some insights for the origin of the particles observed during filter regeneration.

2 Experimental Section

2.1 Drive Cycle, Test Procedure, and Fuel

The drive cycles followed in this study were the US Federal Test Procedure 75 (FTP-75) and the US06 Supplemental Federal Test Procedure (US06). The FTP-75 drive cycle represents typical US city driving conditions and consists of the cold-start, transient, and hot-start phases (Fig. S1; Supplementary Material). The US06 drive cycle represents a more aggressive highway driving condition. Discussions of the drive cycles are given elsewhere [8, 32].

The vehicle prep procedure used in this study is discussed in the Supplementary Material. All tests in this emissions study were conducted using a Tier 2 certification gasoline. Fuel properties and distillation profile of the test fuel are summarized in Tables S1 and S2 (Supplementary Material). The number of valid measurement repeats varies from three to four for each test configuration.

2.2 Emissions Exhaust Characterization Sampling

Vehicular exhaust was diluted using charcoal and high-efficiency particulate air (HEPA)-filtered room air and then introduced into a full-flow constant volume sampling (CVS) dilution tunnel where various gaseous and particle instruments were sampled from. A simplified schematic for the complete exhaust sampling setup is given in Fig. S2, and the operating principles of various instruments are given in the Supplementary Material.

2.3 Test Vehicle and the Gasoline Particulate Filter

The test vehicle used in this study was a 2012 Ford Focus powered by a 2.0-L wall-guided stoichiometric GDI engine. The vehicle was equipped with a TWC. Prior to the emission study, the vehicle had about 6500 km on the odometer. The catalyzed, passive regenerating, wall-flow GPF used in this study was optimized for the current vehicle and the specifications are given in Table S3. The GPF was installed at about 97 cm (38 in.) downstream of the TWC, replacing the original resonator. A series of tests were performed on the same vehicle with the original equipment manufacturer (OEM) resonator instead of the GPF. The maximum differential pressure drops across the GPF over the FTP-75, and US06 drive cycles were about 4.3 and 7.4 kPa, respectively.

Two temperature sensors were installed immediately before and after the GPF. The pre-GPF temperature sensor provides an indication of the exhaust temperature downstream of the TWC (see Fig. S3). For limited runs, two oxygen sensors were installed at positions before and after the GPF to measure the exhaust oxygen concentration (see Fig. S4).

3 Results and Discussion

3.1 Regeneration in Gasoline Particulate Filter

In DPF regeneration, soot oxidation can occur either in the presence of O_2 or a gas mixture of NO_2/O_2. The oxidation of soot by O_2 typically occurs at temperature above 450 °C and is mostly implemented through an active regeneration strategy. Over the typical diesel exhaust temperature range (250–450 °C), oxidation of soot by NO_2/O_2 is more effective and is usually implemented through passive regeneration with the use of a catalyst [33, 34].

For stoichiometric gasoline engines, the concentration of NO downstream of the TWC is expected to be low when compared to the NO emission level from diesel engines. Also, the gasoline exhaust temperature is much higher than that for diesel exhaust. Over the FTP-75 drive cycle, the exhaust temperature at the pre-GPF location was almost always above 500 °C. For the US06 drive cycle, the retained heat generated from the US06 prep (pre-US06) drive cycle and the additional heat generated from the US06 test cycle kept the GPF temperature above 600 °C for most of the time.

Since NO is thermodynamically more stable than NO_2 at high temperatures (e.g., >360 °C) [35], the soot oxidation in the GPF is therefore not likely to rely heavily on NO_2, making the soot oxidation by O_2 the expected pathway. However,

successful GPF regeneration depends heavily on the available oxygen in the gasoline exhaust. A recent study showed that even for a few seconds, duration of fuel cuts during city driving low exhaust temperature condition still represents a mechanism for passive GPF regeneration to occur [24]. To verify this, limited tests were conducted in which the exhaust oxygen concentration was measured (see Fig. S4; Supplementary Material). Prior to the start of the driving, readings from the two oxygen sensors typically agreed to within 1 % and reported about 20 % oxygen, consistent with the oxygen concentration in ambient air. Once the driving began, the exhaust oxygen typically remained zero as one would expect for the stoichiometric combustion condition. However, throughout the drive cycle during deceleration when the fuel supply was cut out, the exhaust oxygen concentration spiked up to ~20 %, similar to the observations reported by Boger et al. [24]. Observations in Fig. S4 point out that there are many occasions throughout both drive cycles when sufficient oxygen is present in the gasoline exhaust to support filter regeneration when the exhaust temperature is high enough. Overall, there are 45 fuel cuts with a median time duration of 20 s in the FTP-75 drive cycle. In comparison, the 20 fuel cuts in the US06 drive cycle have a median duration of 9 s (Table S4).

Over the FTP-75 drive cycle, the post-GPF oxygen concentration during most of the visual spikes is lower than the pre-GPF oxygen concentration by about 1–2 %. Over the middle period of the US06 drive cycle, the difference in oxygen concentration during those spikes reaches up to 5 % or as much as 15 % for the pre-US06 drive cycle. Previous study has shown sequential improvement and deterioration of the particle filtration efficiency of a GPF over the pre-US06 and US06 drive cycles suggesting multiple regenerations occurred over the course of the US06 drive cycle [17]. The oxygen measurements given in Fig. S4 provide further support that soot oxidation occurred in the GPF, and it is suggesting that the biggest consumption of oxygen occurred during the middle period of the pre-US06 drive cycle when the most aggressive driving condition took place. The soot oxidation in the GPF is verified by the temperature measurements, and it is illustrated through two filter regeneration periods indicated in Fig. S3. For example, the 23-s deceleration period A1 in the pre-US06 drive cycle caused a reduction in the pre-GPF exhaust temperature by 67 °C (Table S5). However, the heat released during the exothermic soot regeneration within the same period caused only a drop of 13 °C at the post-GPF location. Similarly, during period B1, the 57-s moderate deceleration caused a reduction in pre-GPF exhaust temperature by 33 °C but the filter regeneration was able to generate enough heat and resulted in a 5 °C increase in post-GPF exhaust temperature at the end of the same period. Similarly, filter regeneration also occurred over the US06 drive cycle (periods A2 and B2). But the increase in temperature caused by the filter regeneration occurred during the pre-US06 drive cycle was larger than that observed during the US06 drive cycle. Therefore, assuming the change in oxygen concentrations and exhaust temperature can be inferred to as the degree of soot oxidation, observations in Fig. S4 suggest that the filter regeneration during the pre-US06 drive cycle was more severe and possibly last longer likely due to the greater amount of pre-deposited soot in the GPF when regeneration occurred. Once most of the deposited soot was consumed, the soot oxidation over the US06 drive cycle was milder despite similar exhaust conditions. At the same time, the oxygen measurements would suggest that there was very limited filter regeneration during the FTP-75 drive cycle.

3.2 Gaseous Emissions and Fuel Consumption

Table 1 summarizes the averaged gaseous emission indices (EIs) and fuel consumption for the vehicle in both the OEM configuration (i.e., stock GDI) and also with the GPF installed (i.e., GDI-GPF). Uncertainties represent 95 % confidence interval error estimates.

CO_2 EIs for the stock GDI and GDI-GPF configurations over both drive cycles were not statistically different based on a 95 % confidence interval as the GPF was optimized in this case. As expected, the emissions of CO, THC, and NO_x for the GDI-GPF configuration showed various degrees of reduction compared to the stock GDI emission levels. Over the FTP-75 drive cycle, the catalyzed GPF provided additional reductions of 86, 38, and 34 % for CO, THC, and NO_x, respectively, when compared to the stock GDI emission levels. It is clear that the reductions were smaller over the cold start (i.e., FTP-75 phase 1) because the catalysts on the GPF had not reached the light-off temperature early enough and were inactive at the early stage of the drive cycle (Fig. S3). Over the US06 drive cycle, emissions of CO, THC, and NO_x for the GDI-GPF configuration were lower than those for the stock GDI configuration by 58, 54, and 88 %, respectively.

The removals of gaseous CO, THC, and NO_x by catalyst are dependent in a complex way on the concentrations of all three compounds [36]. Also, the conversion efficiencies for all three species in the TWC are also functions of the air/fuel ratio [37]. Other factors, such as higher exhaust flow rate and temperature, also play roles during the oxidation of CO and THC. Palladium is known to be able to oxidize NO to NO_2 which aids the soot oxidation [35]. However, NO conversion is thermodynamically limited at higher temperatures [35]. Therefore, soot oxidation by NO_2 should not be a major reason for the reduction of NO_x observed here but still provides one possible removal mechanism for NO_x over the US06 drive cycle.

3.3 Particle Number and Mass Emission Indices

Figures 1 and 2 summarize the averaged EIs for the solid particle number (SPN; both larger than 3 and 23 nm in diameter), PM mass, and black carbon (BC) mass for the stock GDI

Table 1 Gaseous emission indices and fuel consumption (FC) for the stock GDI and GDI-GPF configurations over the FTP-75 (and individual phases) and US06 drive cycles

Vehicle configuration	Stock GDI				
Drive cycle	FTP.ph1	FTP.ph2	FTP.ph3	FTP-75 comp.	US06
CO_2 (g/km)	200.61 ± 5.83	202.88 ± 6.99	167.03 ± 7.02	192.54 ± 6.47	174.10 ± 4.95
CO (g/km)	1.19 ± 0.33	0.52 ± 0.17	0.52 ± 0.10	0.66 ± 0.16	1.05 ± 0.11
NO_x (mg/km)	12.61 ± 2.42	5.90 ± 0.78	19.03 ± 12.62	10.92 ± 3.90	29.33 ± 9.91
THC (mg/km)	24.97 ± 1.09	0.70 ± 0.40	6.47 ± 0.58	7.34 ± 0.24	16.12 ± 2.62
FC (L/100 km)	8.61 ± 0.27	8.66 ± 0.31	7.14 ± 0.30	8.23 ± 0.29	7.39 ± 0.20
Vehicle configuration	GDI-GPF				
Drive cycle	FTP.ph1	FTP.ph2	FTP.ph3	FTP-75 comp.	US06
CO_2 (g/km)	194.63 ± 4.13	196.43 ± 1.84	166.35 ± 4.76	187.76 ± 2.07	176.96 ± 3.79
CO (g/km)	0.30 ± 0.05	0.01 ± 0.00	0.08 ± 0.03	0.09 ± 0.02	0.44 ± 0.10
NOx (mg/km)	11.55 ± 0.83	5.28 ± 1.84	7.40 ± 2.21	7.17 ± 0.98	3.57 ± 0.75
THC (mg/km)	18.01 ± 2.98	0.20 ± 0.26	2.57 ± 0.42	4.55 ± 0.80	7.45 ± 0.70
FC (L/100 km)	8.26 ± 0.17	8.32 ± 0.08	7.05 ± 0.20	7.96 ± 0.09	7.53 ± 0.16

Uncertainties are 95 % confidence interval error estimates

and GDI-GPF configurations over the FTP-75 and US06 (as well as pre-US06) drive cycles. Values are also tabulated in Table 2. Uncertainties are 95 % confidence interval error estimates. Comparing between the stock GDI and GDI-GPF measurements, particle filtration efficiencies over phase 1 of the FTP-75 drive cycle typically varied from 84 to 89 %, regardless of whether PN or PM is used as a measuring matrix. Phases 2 and 3 typically showed filtration efficiencies of 95 % or higher. Over the entire drive cycle, filtration efficiencies of 90 % were typically reached. For the US06 drive cycle, much lower PN and PM filtration efficiencies were observed. For the SPN (>23 nm) or BC mass, a filtration efficiency of about 60 % was reached. The PM mass filtration efficiency was only about 20 %. For SPN (>3 nm), GDI-GPF measurements were higher in magnitude than the stock GDI measurements.

The different PN measurements reveal some interesting facts. For example, the SPN (>3 nm) and SPN (>23 nm) measurements (as well as for PM and BC mass) over the different phases of the FTP-75 drive cycle are in similar magnitude,

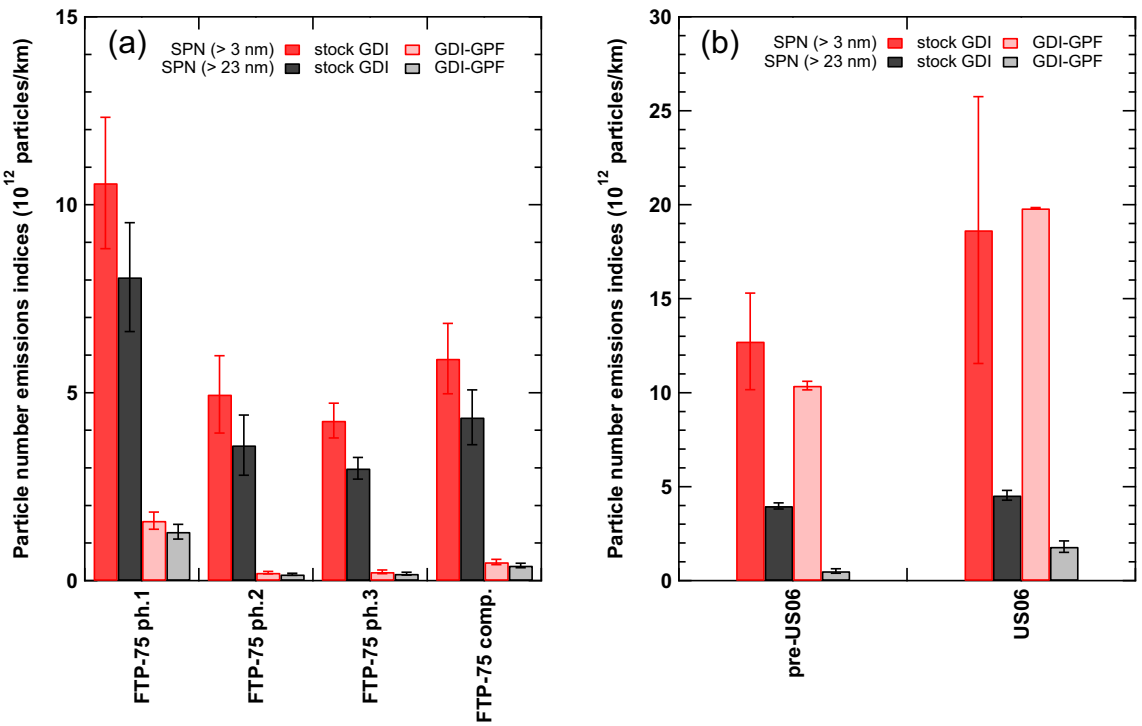

Fig. 1 Comparison of the SPN (>3 nm) and SPN (>23 nm) EIs for **a** the individual phases of the FTP-75 drive cycle as well as the composite average and **b** the pre-US06 and US06 drive cycles for the stock GDI and GDI-GPF configurations

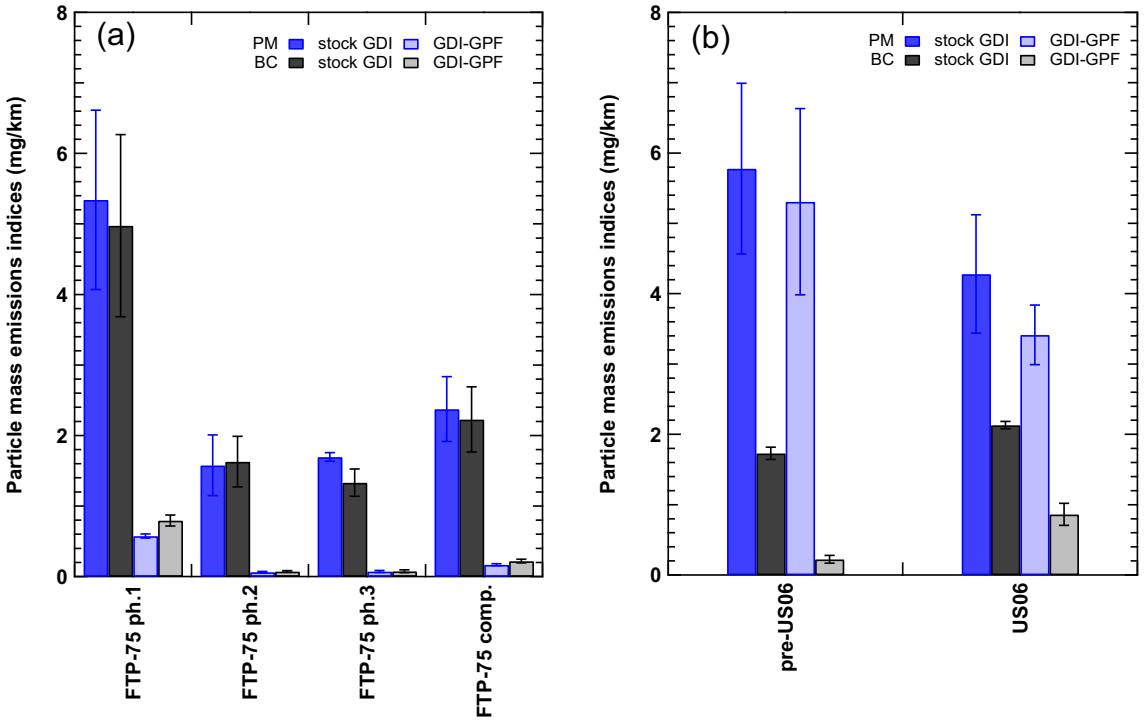

Fig. 2 Comparison of the PM and BC mass EIs over **a** the individual phases of the FTP-75 drive cycle as well as the composite average and **b** the pre-US06 and US06 drive cycles for the stock GDI and GDI-GPF configurations

suggesting that the emitted particles are mostly solid particles and have diameters larger than 23 nm. This is consistent with the TEM results showing particles from all individual phases of the FTP-75 drive cycle having similar solid aggregate structure [31]; selected TEM images are also given in Fig. S10. In contrast, there is a large difference in values between the SPN (>3 nm) and SPN (>23 nm) emissions over the US06 drive cycle suggesting that many of the emitted particles have diameters much smaller than 23 nm, regardless of their origin.

The emission of nanoparticles over the aggressive driving conditions is more complicated. First of all, regardless of the stock GDI or GDI-GPF configuration, the SPN (>23 nm) and BC mass measurements for the pre-US06 and US06 drive cycles are consistent although the US06 post-GPF measurements are higher

Table 2 Particle number (PN), particle mass (PM), and filter-based OC and EC emission indices for the stock GDI and GDI-GPF configurations over the FTP-75 (and individual phases) and US06 drive cycles

Vehicle configuration	Stock GDI				
Drive cycle	FTP.ph1	FTP.ph2	FTP.ph3	FTP-75 comp.	US06
SPN (>3 nm) (10^{12} #/km)	10.57 ± 1.75	4.95 ± 1.03	4.26 ± 0.42	5.91 ± 0.94	18.65 ± 7.10
SPN (>23 nm) (10^{12} #/km)	8.07 ± 1.45	3.60 ± 0.80	2.99 ± 0.29	4.35 ± 0.73	4.54 ± 0.26
PM (mg/km)	5.34 ± 1.27	1.58 ± 0.43	1.70 ± 0.06	2.37 ± 0.46	4.28 ± 0.84
BC (mg/km)	4.98 ± 1.29	1.63 ± 0.36	1.33 ± 0.19	2.23 ± 0.46	2.13 ± 0.05
NIOSH 5040 OC (mg/km)	–	–	–	0.28 ± 0.18	1.93 ± 0.67
NIOSH 5040 EC (mg/km)	–	–	–	2.12 ± 0.64	1.94 ± 0.49
Vehicle configuration	GDI-GPF				
Drive cycle	FTP.ph1	FTP.ph2	FTP.ph3	FTP-75 comp.	US06
SPN (>3 nm) (10^{12} #/km)	1.59 ± 0.23	0.21 ± 0.03	0.23 ± 0.05	0.50 ± 0.07	19.82 ± 8.94
SPN (>23 nm) (10^{12} #/km)	1.30 ± 0.19	0.17 ± 0.03	0.18 ± 0.04	0.40 ± 0.06	1.81 ± 0.30
PM (mg/km)	0.58 ± 0.03	0.06 ± 0.01	0.07 ± 0.02	0.17 ± 0.01	3.42 ± 0.43
BC (mg/km)	0.80 ± 0.08	0.07 ± 0.01	0.08 ± 0.02	0.22 ± 0.03	0.86 ± 0.16
NIOSH 5040 OC (mg/km)	–	–	–	0.04 ± 0.04	1.69 ± 0.77
NIOSH 5040 EC (mg/km)	–	–	–	0.29 ± 0.02	0.99 ± 0.19

Filter-based measurements are integrated results over the entire drive cycle. Uncertainties are 95 % confidence interval error estimates

than the pre-US06 measurements. These measurements suggest that the stock GDI emissions between the pre-US06 and US06 drive cycles were similar. In contrast, the pre-US06 SPN (>3 nm) and PM mass EIs were considerably different compared to their corresponding US06 emissions. For the SPN (>3 nm) EIs, the stock GDI and GDI-GPF emissions over the US06 drive cycle were higher than those from the pre-US06 drive cycle, but for the PM mass EIs, the pre-US06 data were higher in magnitude.

Based on the previous experience from the non-catalyzed GPF work [17], a possible explanation for the higher SPN (>23 nm) and BC mass emissions over the US06 drive cycle than the pre-US06 drive cycle (Figs. S6 and S7) could be due to the reason that filter regeneration began to occur during midway of the pre-US06 drive cycle starting to destroy the soot layer in the GPF. This hypothesis is supported by the real-time SPN (>3 nm) and SPN (>23 nm), as well as the BC and PM mass measurements (Figs. S5–S8). During the initial regeneration stage, rapid fragmentation of pre-deposited soot aggregate could occur, causing some of the particles to pass through the filter in the absence of a soot layer [23, 29]. While the exhaust temperature during the US06 is much higher than for the FTP-75, the supply of oxygen during fuel cuts for soot oxidation is less frequent during the US06 drive cycle (Table S4). This could potentially lead to incomplete combustion of the deposited soot, leading to the emissions of organic materials which could contribute to PM mass but not necessarily to BC mass [31]. The lack of a developed soot layer to remove the BC particles causes the GDI-GPF BC EIs over the US06 drive cycle to be slightly higher than those over the pre-US06 drive cycle.

The observations of the SPN (>3 nm) measurements are more complicated. Some studies suggested that PN measurements for particles smaller than 23 nm under the PMP protocol may be attributed to artifact because the volatile particles may not be completely evaporated and the PMP system may not totally suppress the appearance of the nanoparticles smaller than 23 nm [38–40]. However, the SPN (>3 nm) measurements generally correlate well with the PN emissions obtained from the size distributions measured downstream of the thermodenuder (with a correlation coefficient varying from 0.87 to 0.97; Supplementary Material). Therefore, it is possible that some of the nanoparticles could be formed as a result of the adsorption of hot gaseous materials onto the walls of the transfer line and in the CVS over the pre-US06 drive cycle which then caused nucleation in the CVS over the subsequent US06 test [41]. If the residence time inside the thermodenuder is not long enough to completely evaporate the semi-volatile particles, the vapor cannot be effectively removed by the activated charcoal [42, 43], causing nanoparticles to be measured as part of the size distributions.

3.4 Real-Time PN and PM Emissions Over the FTP-75

Figure 3a shows the real-time cumulative SPN (>3 nm) and SPN (>23 nm) emissions for both the stock GDI and GDI-GPF configurations over the FTP-75 drive cycle whereas Fig. 3b shows the corresponding PM and BC mass measurements over the same drive cycle. Both the cumulative SPN (>3 nm) and SPN (>23 nm) emissions increase gradually over the course of the drive cycle suggesting continuous emissions of particles even from a warmed GDI engine. The cold-start emissions represent a significant fraction of the total emitted particles over the entire drive cycle. For example, the cumulative SPN (>3 nm) and SPN (>23 nm) emissions at the end of the FTP-75 phase 1 represent 52 and 54 % of the total emissions, respectively, over the entire cycle. The real-time SPN measurements over the FTP-75 drive cycle were also highly repeatable as illustrated in Figs. S5 and S6. The similar magnitude between the SPN (>3 nm) and SPN (>23 nm) measurements confirm that most of the emitted particles have diameters above 23 nm, and the emissions of nanoparticles over the FTP-75 drive cycle from the GDI vehicle were low.

As the primary filtration mechanism for a wall-flow filter is attributed mostly to the soot cake filtration from the accumulated soot in the filter, how rapid a GPF can achieve high particle filtration efficiency depends on the time required to condition the GPF. The cumulative stock GDI SPN (>3 nm) and SPN (>23 nm) measurements (Fig. 3a) reached 80 % of the final values at about 1405 and 1260 s, respectively, from the start of the cycle. In contrast, the cumulative GDI-GPF SPN (>3 nm) and SPN (>23 nm) reached 80 % of their corresponding final values at about 655 and 527 s from the start of the cycle, suggesting that a GPF can be optimized such that it does not require a long period of time to condition before achieving high filtration efficiency. Once the GPF is conditioned, particle emissions downstream of the GPF remained low even though there were continuous particle emissions from the engine.

The PM and BC mass emissions over the FTP-75 drive cycle (Fig. 3b) mimic the SPN (>3 nm) and SPN (>23 nm) emission patterns. The real-time emissions (Figs. S7 and S8) were also highly repeatable. All these measurements support the fact that most of the emitted particles from the GDI engine over the FTP-75 drive cycle can be attributed to the solid soot particles, i.e., these freshly emitted particles do not contain an appreciable amount of semi-volatile materials. The filter-based OC/EC also provided further support to this conclusion (Table 2). For the stock GDI configuration, the EC EI over the entire FTP-75 drive cycle was determined to be about 2.1 mg/km, compared well with the composite average of 2.2 mg/km BC EI. After correcting for positive filter artifact, the OC EI was determined to be 0.3 mg/km, suggesting that EC contributed about 88 % of the total carbonaceous mass. This percentage could be slightly lower after considering other non-carbonaceous mass, such as hydrogen and oxygen, which cannot be determined through the thermal/optical analysis, though the non-

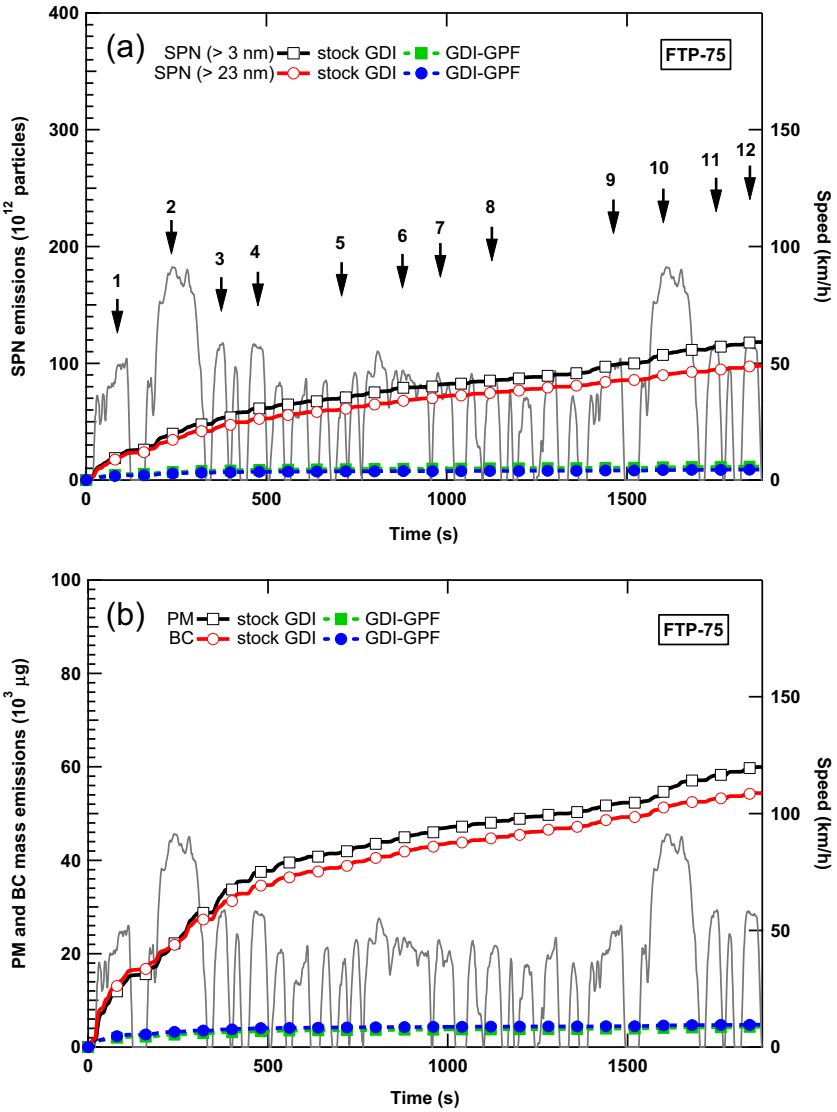

Fig. 3 Real-time cumulative **a** SPN (>3 nm) and SPN (>23 nm) emissions and **b** PM and BC mass emissions for the stock GDI and GDI-GPF configurations over the FTP-75 drive cycle. For presentation purpose, the hot soak between phases 2 and 3 is removed. The *arrows* in **a** show the approximate locations where number size distributions were extracted and illustrated in Fig. 5

carbonaceous mass from freshly emitted GDI soot particles is expected to be low. Nonetheless, the EC fraction in carbonaceous mass is consistent with the 94 % BC fraction in PM from real-time measurements.

For the GDI-GPF measurements over the FTP-75 drive cycle, the OC/EC measurements suggest that EC contributes roughly 88 % of all the carbonaceous mass. For the real-time measurements, both BC and PM measurements were close to their respective detection limits with similar magnitude, suggesting that particles were primarily made up of BC. Also note that the BC and PM results obtained from the real-time instruments were derived primarily based on fine particles. Some much larger accumulation mode particles, which may or may not have exactly the same composition as the fine particles, could also be collected on filters and influence the OC/EC results. Regardless, these results all point to the same direction that the particles collected from the stock GDI and GDI-GPF configurations could share similar composition.

The fact that particles measured from the stock GDI and GDI-GPF configuration over the FTP-75 drive cycle have similar composition may not be a total surprise. Detail TEM image analyses showed that the two groups of particles have very comparable morphology, and they are not statistically different implying that they are likely to be the same type of particles (Fig. S10) [31]. The size distribution measurements, which will be shown in the coming section, indeed suggest that these are the same group of particles which appear downstream of the GPF because they cannot be removed completely by the filter due to the fact that these particles have diameters that lie in the region where the minimum filtration efficiency of the filter occurs [44].

3.5 Real-Time PN and PM Emissions Over the US06

The cumulative PN and PM emissions for the stock GDI and GDI-GPF configurations over the US06 drive cycle are summarized in Fig. 4a, b. Interestingly, the SPN (>23 nm) and BC emissions for both the stock GDI and GDI-GPF configurations all increased gradually over the course of the cycle and never reach a plateau. These observations imply that the GPF was not able to be conditioned over the exhaust conditions encountered during the US06 drive cycle, and the particle filtration efficiency for the solid particles remained low. At the same time, the SPN (>3 nm) and PM emissions for both stock GDI and GDI-GPF configurations all increased sharply near the midway point of the drive cycle. The increases in emissions for the stock GDI configuration suggest that additional nanoparticles could be emitted from the GDI vehicle in addition to the solid soot particles under very aggressive driving conditions. The increases in SPN (>3 nm) and PM mass for the GDI-GPF configuration indicate a possible filter regeneration event which is clearly supported by the real-time PN measurements in Fig. S5(f). In addition, the data also suggest possible formation of new particles downstream of the GPF.

The contrasting patterns between the cumulative SPN (>3 nm) and SPN (>23 nm) emissions in the GDI-GPF configuration suggest that the additional particles observed during the filter regeneration were primarily nanoparticles with diameters less than 23 nm and were likely formed downstream of the GPF when the exhaust temperature is cooled in the CVS. In this case, the appearance of the nanoparticles downstream of the GPF did not contribute a significant amount to PM mass since most of the PM mass was attributed to the accumulation mode particles which the GPF still provided certain degree of filtration. The real-time measurements show that the GPF reduced BC EIs from 2.1 to 0.9 mg/km, giving an average filtration efficiency of about 60 %. The PM EIs reduced from 4.3 to 3.4 mg/km with the use of a GPF, showing only a 20 % reduction due to the formation of new semi-volatile particles

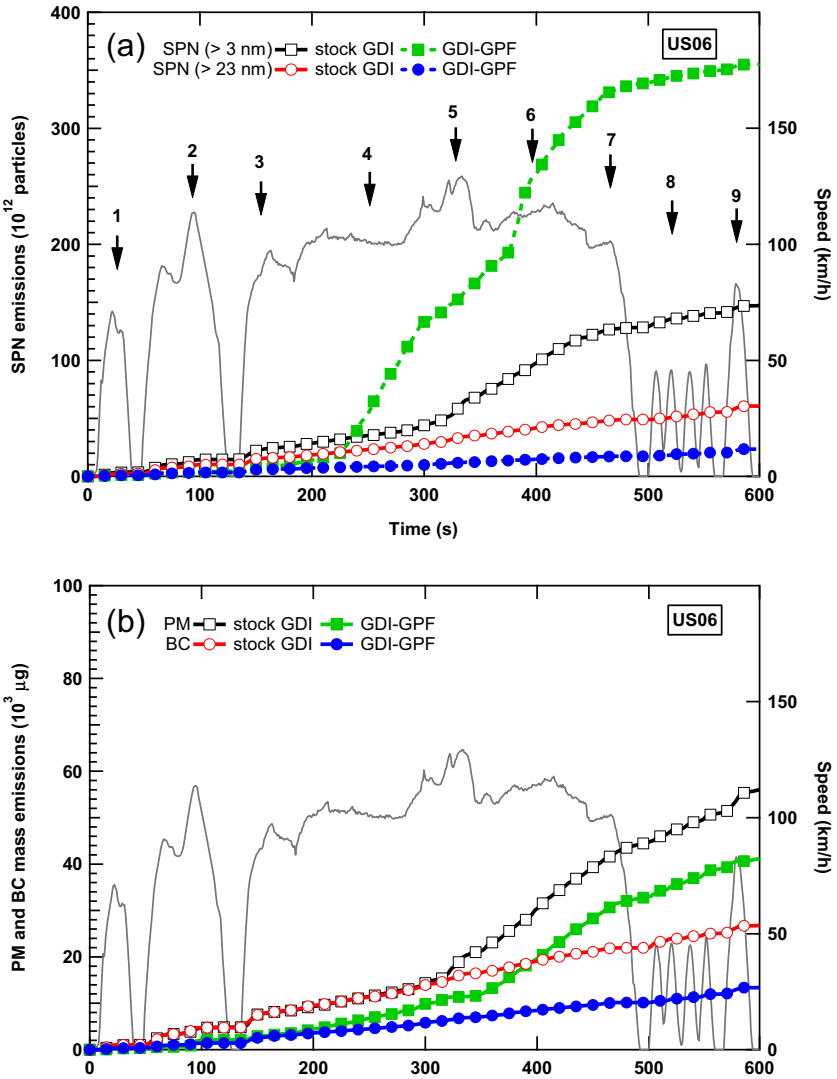

Fig. 4 Real-time cumulative **a** SPN (>3 nm) and SPN (>23 nm) emissions and **b** PM and BC mass emissions for the stock GDI and GDI-GPF configurations over the US06 drive cycle. The *arrows* in **a** show the approximate locations where number size distributions were extracted and illustrated in Fig. 6

during filter regeneration. These measurements suggest that BC contributes about 50 % of the emitted particles during the stock GDI configuration and only 25 % during filter regeneration. The EC EIs for the stock GDI (1.9 mg/km) and GDI-GPF (1.0 mg/km) configurations over the US06 drive cycle were also consistent with the BC EIs (Table 2), suggesting that EC contributes roughly 50 and 37 % of the carbonaceous mass for the stock GDI and GDI-GPF conditions, respectively.

The increase in organic fraction in the emitted PM during filter regeneration was also captured by the TEM images (Fig. S10(f)). In this case, the pre-existing soot particles provide some surfaces for the semi-volatile materials to adsorb or condense onto, thereby forming a layer of coating on the soot aggregates. The coating was not enough to completely enclose the soot aggregates and, therefore, did not significantly change the fractal dimension but enough to blur the boundaries of the primary soot particles causing a 20 % increase in the size of the primary particle when viewed under the TEM [31]. In addition, the TEM images also show some small and droplet-like structures in the background, which are consistent with the observation of nanoparticle emissions. These small particles appear translucent to the electron beam, implying that they are primarily composed of semi-volatile materials [31], supporting the high amount of OC identified from the quartz filters (Table 2).

3.6 Particle Number Size Distributions

To understand the particle emission characteristics over the stock GDI and GDI-GPF configurations, the particle number size distributions measured during various degrees of

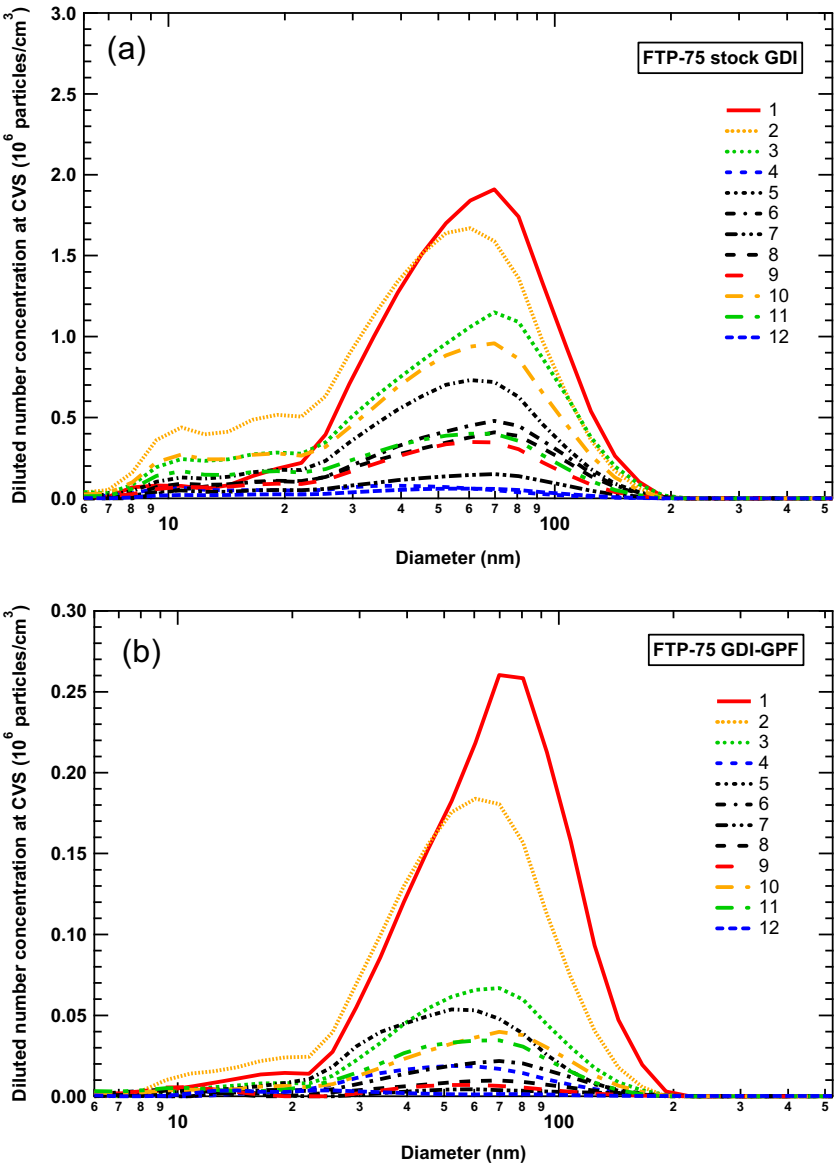

Fig. 5 Particle number size distributions extracted at various moments (*arrows* in Fig. 3a) over the FTP-75 drive cycle for the **a** stock GDI and **b** GDI-GPF configurations

accelerations over the two drive cycles (indicated by the arrows in Figs. 3a and 4a) were extracted and compared. Figure 5a, b summarize the size distributions measured at various moments over the FTP-75 drive cycle for the stock GDI and GDI-GPF configurations, respectively. Some of the distributions in the Figures are colored to improve the visual presentation and comparison. All size distribution measurements represent the diluted concentration in the CVS tunnel. These data show that the particle number size distributions measured throughout various driving conditions in the FTP-75 drive cycle were very similar in shape, but the absolute concentrations were influenced by the vehicle operating condition. There are periods (e.g., ~229 s; scan 2) when a small number of particles with diameter less than or equal to 30 nm (i.e., nanoparticles) were also co-emitted, but in most cases, the majority of the particles were about 50–90 nm in diameter.

Particles measured downstream of the GPF were also in the diameter range of 50–90 nm. In general, the particle number concentrations measured downstream of the GPF were an order of magnitude lower than those for stock GDI levels. In addition, the GDI-GPF size distributions showed a clear progressive reduction in number concentration over time when compared to the stock GDI measurements at the same corresponding moments. For example, at 93 s from the start of the FTP-75 drive cycle (i.e., scan 1), the ratio of the peak concentration of the stock GDI size distribution to the peak concentration of the GDI-GPF distribution was about 7. At 373 s (i.e., scan 3), this ratio increased to 17. By 1600 s (i.e., scan 10), this ratio was 24, showing a significant improvement in the particle filtration efficiency over time.

The particle number size distributions over the US06 drive cycle were very different from those measured during the

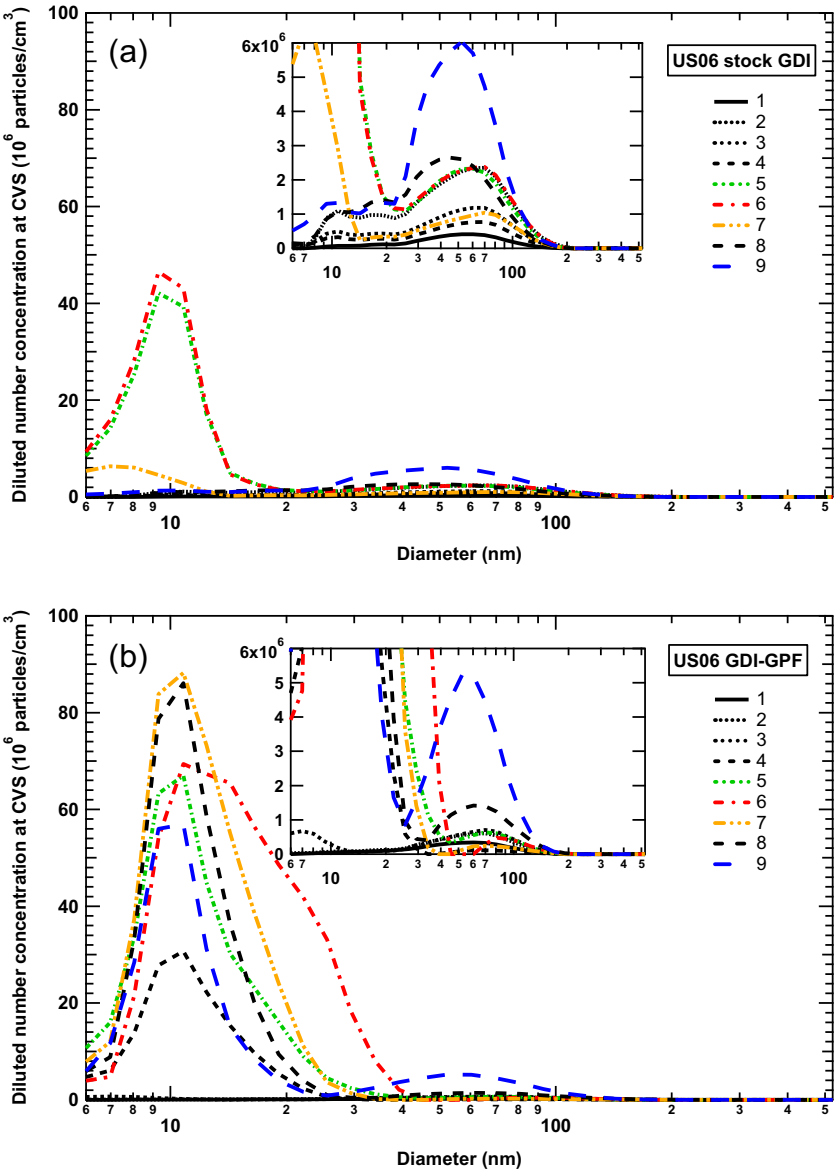

Fig. 6 Particle number size distributions extracted at various moments (*arrows* in Fig. 4a) over the US06 drive cycle for the **a** stock GDI and **b** GDI-GPF configurations

FTP-75 drive cycle. For the stock GDI configuration (Fig. 6a), there was evidence of the emissions of the accumulation mode particles (40–90 nm). But whenever a bimodal distribution was observed, the nanoparticles (<20 nm) were completely dominating in number compared to the accumulation mode particles. Nanoparticles were emitted during more aggressive driving conditions, such as from 300 to 500 s from the start of the cycle (i.e., scans 5–7). The appearance of these nanoparticles is also clearly illustrated by the elevation of the SPN (>3 nm) time series (Fig. S5(e)) compared to the SPN (>23 nm) time series (Fig. S6(e)) which occurs around the similar time interval.

The GDI-GPF size distributions over the US06 drive cycle (Fig. 6b) also reveal additional insights. First of all, it is evident that the number concentration for the 40–90 nm accumulation mode particles is lower than that of the stock GDI configuration suggesting that the GPF still provides a certain degree of filtration for these solid particles despite the continued regeneration of the GPF. Starting from about 250 s onwards (i.e., scan 4 onwards), a large number of nanoparticles with diameters less than 30 nm were emitted regardless of the driving conditions. In many cases, the number concentrations for these nanoparticles were much higher compared to the concentrations measured during the stock GDI configuration, implying that these nanoparticles were not emitted from the engine.

The nanoparticles and accumulation mode particles did not have any apparent relationship, and they represent two separate groups of particles generated likely from different physical processes. The emissions of the nanoparticles are clearly illustrated by the SPN (>3 nm) time series (Fig. S5(f)) and are consistent with other reported emissions during filter regeneration [20, 21]. The accumulation mode particles appear to be the particles that are not completely filtered out by the relatively thin or undeveloped soot layer in the GPF because these particles are typically too large to be removed by diffusion and too small to be removed by impaction or interception in the GPF. These particles are in the similar size range when compared to the (60–150 nm) particles that have minimum filtration efficiencies from a non-catalyzed GPF investigated in the previous stage of the program [17] and are also close to the particle diameter range predicted to have the minimum filtration efficiency through filter [44].

3.7 Implications

This work shows that the solid and BC particle emissions from emerging GDI vehicles can be readily reduced with the use of a GPF. Although the effective removal of particles in a GPF relies heavily on the buildup of a soot layer in the filter, this work also shows that even a clean filter can still provide a certain degree of filtration for BC particles. Once optimized, a wall-flow GPF can potentially reach over 90 % filtration efficiency within a short period of time without significantly increasing the fuel consumption of the vehicle. By incorporating catalyst materials in the GPF, additional reduction in CO, THC, and NO_x emissions can also be achieved compared to the stock GDI configuration. Over the aggressive highway driving conditions, filter regeneration was observed during which a lot of nanoparticles were formed downstream of the GPF. These nanoparticles are typically smaller than 30 nm in diameter and are potentially made up of semi-volatile materials as inferred from TEM measurements. Further research is needed to fully characterize the composition and nature of these particles and to understand the environmental and human health implications when released into the atmosphere. The filter regeneration was not observed or was not significant over moderate city driving conditions exhibited during the FTP-75 drive cycle. Considering that GDI engines can still emit an observable number of solid particles during moderate driving conditions, the use of a GPF can be employed to reduce emissions of BC particles from GDI vehicles in areas where moderate driving condition is expected.

Acknowledgments The authors would like to acknowledge the Emission Research and Measurement Section (ERMS) staff for their assistance in conducting this vehicle emission research project. Financial support was provided by the Government of Canada's Program of Energy Research and Development (PERD) Projects AFTER10 and AFTER11. The test vehicle was provided by Transport Canada through the eTV program. The prototype GPF was provided by Manufacturers of Emission Controls Association (MECA).

References

1. Bond, T.C., Doherty, S.J., Fahey, D.W., Forster, P.M., Bemtsen, T., DeAngelo, B.J., Flanner, M.G., Ghan, S., Kärcher, B., Koch, D., Kinne, S., Kondo, Y., Quinn, P.K., Sarofim, M.C., Schultz, M.G., Schulz, M., Venkataraman, C., Zhang, H., Zhang, S., Bellouin, N., Guttikunda, S.K., Hopke, P.K., Jacobson, M.Z., Kaiser, J.W., Klimont, Z., Lohmann, U., Schwarz, J.P., Shindell, D., Storelvmo, T., Warren, S.G., Zender, C.S.: Bounding the role of black carbon in the climate system: a scientific assessment. J. Geophys. Res. Atmos. **118**, 5380–5552 (2013)
2. Japar, S.M., Brachaczek, W.W., Gorse Jr., R.A., Norbeck, J.M., Pierson, W.R.: The contribution of elemental carbon to the optical properties of rural atmospheric aerosols. Atmos. Environ. **20**, 1281–1289 (1986)
3. Wilker, E.H., Baccarelli, A., Suh, H., Vokonas, P., Wright, R.O., Schwartz, J.: Black carbon exposures, blood pressure, and interactions with single nucleotide polymorphisms in microRNA processing genes. Environ. Health Perspect. **118**(7), 943–948 (2010)
4. Zhao, F., Lai, M.C., Harrington, D.L.: Automotive spark-ignited direct-injection gasoline engines. Prog. Energy Combust. Sci. **25**, 437–562 (1999)
5. Alkidas, A.C.: Combustion advancements in gasoline engines. Energy Convers. Manag. **48**, 2751–2761 (2007)
6. He, X., Ratcliff, M.A., Zigler, B.T.: Effects of gasoline direct injection engine operating parameters on particle number emissions. Energy Fuel **26**, 2014–2027 (2012)

7. Barone, T.L., Storey, J.M.E., Youngquist, A.D., Szybist, J.P.: An analysis of direct-injection spark-ignition (DISI) soot morphology. Atmos. Environ. **49**, 268–274 (2012)
8. Chan, T.W., Meloche, E., Kubsh, J., Brezny, R.: Black carbon emissions in gasoline exhaust and a reduction alternative with a gasoline particulate filter. Environ. Sci. Technol. **48**, 6027–6034 (2014)
9. Sementa, P., Vaglieco, B.M., Catapano, F.: Thermodynamic and optical characterizations of a high performance GDI engine operating in homogeneous and stratified charge mixture conditions fueled with gasoline and bio-ethanol. Fuel **96**, 204–219 (2012)
10. Maricq, M.M., Szente, J.J., Adams, J., Tennison, P., Rumpsa, T.: Influence of mileage accumulation on the particle mass and number emissions of two gasoline direct injection vehicles. Environ. Sci. Technol. **47**, 11890–11896 (2013)
11. Aikawa, K., Sakurai, T., Jetter, J.J.: Development of a predictive model for gasoline vehicle particulate matter emissions. SAE Int. J. Fuels Lubr. **3**(2), 610–622 (2010). doi:10.4271/2010-01-2115
12. Khalek, I.A., Bougher, T., Jetter, J.J.: Particle emissions from a 2009 gasoline direction injection engine using different commercially available fuels. SAE Int. J. Fuels Lubr. **3**(2), 623–637 (2010). doi:10.4271/2010-01-2117
13. Botero, M.L., Mosbach, S., Kraft, M.: Sooting tendency of paraffin components of diesel and gasoline in diffusion flames. Fuel **126**, 8–15 (2014)
14. Chan, T.W.: The impact of isobutanol and ethanol on gasoline fuel properties and black carbon emissions from two light-duty gasoline vehicles, SAE Tech. Paper, 2015-01-1076 (2015)
15. Karavalakis, G., Short, D., Vu, D., Russell, R., Hajbabaei, M., Asa-Awuku, A., Durbin, T.D.: Evaluating the effects of aromatics content in gasoline on gaseous and particulate matter emissions from SI-PFI and SIDI vehicles. Environ. Sci. Technol. **49**, 7021–7031 (2015)
16. Saito, C., Nakatani, T., Miyairi, Y., Yuuki, K., Makino, M., Kurachi, H., Heuss, W., Kuki, T., Furuta, Y., Kattouah, P. Vogt, C.D.: New particulate filter concept to reduce particle number emissions, SAE Tech. Paper, 2011-01-0814 (2011)
17. Chan, T.W., Meloche, E., Kubsh, J., Rosenblatt, D., Brezny, R., Rideout, G.: Evaluation of a gasoline particulate filter to reduce particle emissions from a gasoline direct injection vehicle. SAE Int J. Fuels Lubr. **5**(3), 1277–1290 (2012). doi:10.4271/2012-01-1727
18. Chan, T.W., Meloche, E., Kubsh, J., Brezny, R., Rosenblatt, D., Rideout, G.: Impact of ambient temperature on gaseous and particle emissions from a direct injection gasoline vehicle and its implication on particle filtration. SAE Int. J. of Fuels Lubr. **6**(2), 350–371 (2013). doi:10.4271/2013-01-0527
19. Richter, J.M., Klingmann, R., Spiess, S., Wong, K.F.: Application of catalyzed gasoline particulate filters to GDI vehicles. SAE Int. J. Engines **5**(3), 1361–1370 (2012). doi:10.4271/2012-01-1244
20. Bikas, G., Zervas, E.: Regulated and non-regulated pollutants emitted during the regeneration of a diesel particulate filter. Energy Fuel **21**, 1543–1547 (2007)
21. Barone, T.L., Storey, J.M.E., Domingo, N.: An analysis of field-aged diesel particulate filter performance: particle emissions before, during, and after regeneration. J. Air Waste Manag. Assoc. **60**, 968–976 (2010)
22. Zhong, D., He, S., Tandon, P., Moreno, M., Boger, T.: Measurement and prediction of filtration efficiency evolution of soot loaded diesel particulate filters, SAE Tech. Paper, 2012-01-0363 (2012)
23. Cauda, E., Hernandez, S., Fino, D., Saracco, G., Specchia, V.: PM0.1 emissions during diesel trap regeneration. Environ. Sci. Technol. **40**, 5532–5537 (2006)
24. Boger, T., Rose, D., Nicolin, P., Gunasekaran, N., Glasson, T.: Oxidation of soot (Printex® U) in particulate filters operated on gasoline engines. Emission Cont. Sci. Technol. **1**, 49–63 (2015)
25. Abdul-Khalek, I.S., Kittelson, D.B., Brear, F.: Diesel trap performance: particle size measurements and trends, SAE Tech. Paper, 982599 (1998)
26. Matter, U., Siegmann, H.C., Kasper, M., Burtscher, H.: Distinction of volatile and nonvolatile particles in exhaust of diesel engines with particulate traps. J. Aerosol Sci. **30**, S471–S472 (1999)
27. Vaaraslahti, K., Virtanen, A., Ristimäki, J., Keskinen, J.: Nucleation mode formation in heavy-duty diesel exhaust with and without a particulate filter. Environ. Sci. Technol. **38**, 4884–4890 (2004)
28. Zhao, H., Ge, Y., Wang, X., Tan, J., Wang, A., You, K.: Effects of fuel sulfur content and diesel oxidation catalyst on PM emitted from light-duty diesel engine. Energy Fuel **24**, 985–991 (2010)
29. Konstandopoulos, A.G., Melas, A., Baltzopoulou, P., Vlachos, N., Kostoglou, M. : Soot deposit evolution and the mechanism of particle emissions during regeneration in diesel particulate filters, in Proceeding of the 19th ETH Conference on Combustion Generated Nanoparticles, June 28-July 1, Zürich, Switzerland (2015)
30. Dwyer, H., Ayala, A., Zhang, S., Collins, J., Huai, T., Herner, J., Chau, W.: Emissions from a diesel car during regeneration of an active diesel particulate filter. J. Aerosol Sci. **41**, 541–552 (2010)
31. Saffaripour, M., Chan, T.W., Liu, F., Thomson, K.A., Smallwood, G.J., Kubsh, J., Brezny, R.: Effect of drive cycle and gasoline particulate filter on the size and morphology of soot particles emitted from a gasoline-direct-injection vehicle. Environ. Sci. Technol. 49, 11950–11958 (2015). doi:10.1021/acs.est.5b02185
32. Kamboures, M.A., Hu, S., Yu, Y., Sandoval, J., Rieger, P., Huang, S.M., Zhang, S., Dzhema, I., Huo, D., Ayala, A., Chang, M.C.O.: Black carbon emissions in gasoline vehicle exhaust: a measurement and instrument comparison. J. Air Waste Manag. Assoc. **63**(8), 886–901 (2013)
33. Stanmore, B.R., Brilhac, J.F., Gilot, P.: The oxidation of soot: a review of experiments, mechanisms and models. Carbon **39**, 2247–2268 (2001)
34. Jeguirim, M., Tschamber, V., Ehrburger, P.: Catalytic effect of platinum on the kinetics of carbon oxidation by NO2 and O2. Appl. Catal. B Environ. **76**, 235–240 (2007)
35. Majewski, W.A., Ambs, J.L., and Bickel, K. (1995). Nitrogen oxides reactions in diesel oxidation catalyst, SAE Technical Paper, 950374
36. Heywood, J.B.: In: Duffy, A., Morriss, J.M. (eds.) Pollutant Formation and Control in: Internal Combustion Engine Fundamental, chapter, 11 567–660. McGraw-Hill, Inc, New York (1988)
37. Heck, R.M., Farrauto, R.J.: Automobile exhaust catalysts. Appl. Catal. A Gen. **221**, 443–457 (2001)
38. Giechaskiel, B., Mamakos, A., Andersson, J., Dilara, P., Martini, G., Schindler, W., Bergmann, A.: Measurement of automotive nonvolatile particle number emissions within the European legislative framework: a review. Aerosol Sci. Technol. **46**, 719–749 (2012)
39. Johnson, K.C., Durbin, T.D., Jung, H., Chaudhary, A., Cocker III, D.R., Herner, J.D., Robertson, W.H., Huai, T., Ayala, A., Kittelson, D.: Evaluation of the European PMP methodologies during on-road and chassis dynamometer testing for DPF equipped heavy-duty diesel vehicles. Aerosol Sci. Technol. **43**, 962–969 (2009)
40. Zheng, Z., Johnson, K.C., Liu, Z., Durbin, T., Hu, S., Huai, T., Kittelson, D.B., Jung, H.S.: Investigation of solid particle number measurement: existence and nature of sub-23 nm particles under PMP methodology. J. Aerosol Sci. **42**, 883–897 (2011)
41. Maricq M.M., Chase R.E., Podsiadlik D.H., Vogt R.: Vehicle exhaust particle size distributions: a comparison of tailpipe and dilution tunnel measurements, SAE Tech. Paper, 1999-01-1461 (1999)
42. Wehner, B., Philippin, S., Wiedensohler, A.: Design and calibration of a thermodenuder with an improved heating unit to measure the size-dependent volatile fraction of aerosol particles. J. Aerosol Sci. **33**, 1087–1093 (2002)

43. Park, D., Kim, S., Choi, N.K., Hwang, J.: Development and performance test of a thermo-denuder for separation of volatile matter from submicron aerosol particles. J. Aerosol Sci. **39**, 1099–1108 (2008)

44. Hinds, W.C.: Aerosol technology: properties, behaviour, and measurement of airborne particles. In: Filtration. chapter 9, 2nd edn, pp. 182–205. Wiley, Toronto (1999)